journal

J. Am. Ceram. Soc., **88** [6] 1584–1590 (2005)
DOI: 10.1111/j.1551-2916.2005.00296.x

Co-Doping of Air Plasma-Sprayed Yttria- and Ceria-Stabilized Zirconia for Thermal Barrier Applications

Zun Chen and Rodney Trice[†]

School of Materials Engineering, Purdue University, West Lafayette, Indiana 47907-2044

Hsin Wang, Wally Porter, and Jane Howe

Oak Ridge National Laboratory Oak Ridge, Tennessee 37831-6087

Matthew Besser and Daniel Sordelet

Ames Laboratory, Iowa State University, Ames, Iowa 50011

Co-dopants of either Yb^{3+} or Ca^{2+} were incorporated into 7.6 mol% $YO_{1.5}$–ZrO_2 (7.6YSZ) and 12 mol% CeO_2–ZrO_2 (12CeSZ) coatings by infiltrating porous spray-dried powders with salt solutions containing the appropriate co-dopant species prior to plasma spraying. Co-dopant concentration was varied from 2 to 5 mol%. Using a combination of transmission electron microscopy and energy-dispersive analysis, no secondary phase or Yb^{3+} segregation was detected at the grain boundary of either as-sprayed 2Yb/7.6YSZ or 2Yb/12CeSZ coatings. Dilatometer measurements showed that 2 mol% Yb^{3+} co-doped 7.6YSZ and 12CeSZ coatings shrank ~0.6% during a 5 h soak at 1400°C, approximately the same contraction as the baseline coatings (i.e. not co-doped). X-ray diffraction results show that the as-sprayed 7.6YSZ, 2Ca/7.6YSZ, and 2Yb/7.6YSZ coatings comprised of non-transformable, non-equilibrium composition tetragonal ZrO_2 (identified presently as t'-ZrO_2), while the 5Ca/7.6YSZ coating was a non-equilibrium composition of cubic ZrO_2. After a heat treatment of 100 h at 1200°C, the 2Yb/7.6YSZ coating was completely t'-ZrO_2, while the baseline and Ca^{2+} co-doped 7.6YSZ coatings showed evidence of partitioning. Therefore, it appears that co-doping of 7.6YSZ with 2 mol% Yb^{3+} increases the stability of t'-ZrO_2, whereas co-doping with 2 mol% Ca^{2+} decreases the stability of t'-ZrO_2. The volume fraction of m-ZrO_2 in the baseline 12CeSZ coatings was estimated to be 88% after a 100 h heat treatment at 1200°C. 2 mol% Yb^{3+} or Ca^{2+} co-doping limited the tetragonal to monoclinic phase transformation in 12CeSZ, with only 37% and 43% monoclinic phase observed, respectively, after a 100 h heat treatment at 1200°C; this was an improvement over the baseline 12CeSZ coating. As-sprayed 2Yb/7.6YSZ and 2Yb/12CeSZ coatings had slightly lower thermal conductivity than their baseline counterparts in the as-sprayed condition; after 100 h at 1200°C, their conductivity increased to that of the baseline coatings.

I. Introduction

VIRTUALLY every aircraft flying today uses thermal barrier coatings (TBCs) to protect metallic components within the gas turbine engine from temperature extremes and to allow them to operate at higher temperatures, thus increasing the overall operating efficiency. A TBC typically consists of two layers, e.g., a ~200 μm thick zirconia-based topcoat and a ~100 μm metallic bond coat (MCrAlY, where M can be Co, Ni, or Fe).[1] The zirconia layer is most often stabilized with Y_2O_3, but other oxides, like CeO_2, have been suggested.[2,3] These coatings can be applied via electron beam physical vapor deposition or plasma spray; the latter is the focus in the current work.

While TBCs are widely used to increase the durability of hot section components in land-based gas turbines used for power generation,[4,5] durability and reliability issues limit the benefits that can be derived from their use.[6] For example, the change in phase assemblage of the zirconia topcoat after multiple hours at temperatures at or above 1200°C can limit their durability. X-ray analysis of as-sprayed 7.6 mol% $YO_{1.5}$–ZrO_2 (7.6YSZ) coatings at room temperature reveals a single metastable tetragonal zirconia phase (referred to presently as t'-ZrO_2), with a composition of 7.6 mol% $YO_{1.5}$,[7] rather than m-ZrO_2 and c-ZrO_2,[8] as would be predicted by the phase diagram. However, this metastable t'-ZrO_2 phase is favored in TBC applications because of its high cyclic life.[9] The problem with this metastable phase is that it tends to partition into equilibrium composition t-ZrO_2 (~4 mol% $YO_{1.5}$) and c-ZrO_2 (~14 mol% $YO_{1.5}$) phases during long durations at high temperatures. Upon cooling, the now equilibrium composition of t-ZrO_2 will transform to m-ZrO_2, resulting in cracking of the coating. Ilavsky and Stalick[10] confirmed the partitioning of the t'-ZrO_2 phase after heat treatment at temperatures of 1100°–1400°C using neutron diffraction. Another study by Ilavsky *et al.*[11] showed that as the yttria content in the tetragonal phase approached a limiting concentration, the t-ZrO_2 phase would transform into m-ZrO_2 phase on cooling.

Lee *et al.*[12] studied the phase transformations of plasma-sprayed ZrO_2–CeO_2 (with 12–20.1 mol% CeO_2) TBCs. They found that as-sprayed CeSZ coatings with 12 and 13.6 mol% CeO_2 consisted of a single non-equilibrium t'-ZrO_2, while those with 15.2–20.1 mol% CeO_2 contained a mixture of t'-ZrO_2 and c'-ZrO_2 phases. During 45 min cyclic oxidation at 1135°C, the non-equilibrium t'-ZrO_2 and c'-ZrO_2 partitioned into the equilibrium t-ZrO_2 and c-ZrO_2 phases. Some of the tetragonal phases transformed to the monoclinic phase during cooling.

As the formation of m-ZrO_2 typically results in cracking of the coating, limiting the partitioning of the non-equilibrium phases that result during plasma spraying may lead to increased life in TBCs. Rebollo *et al.*[13] recently studied the phase stability

R. S. Hay—contributing editor

Manuscript No. 11277. Received August 18, 2004; approved December 7, 2004.

Part of this research effort was supported by a grant form the California Energy Commission, Grant # 51979A/00-22. The work performed at Ames Laboratory was supported by the U.S. Department of Energy through Iowa State University under Contract No. W-7405-ENG-82.

Research sponsored by the Assistant Secretary for Energy Efficiency and Renewable Energy, Office of FreedomCAR and Vehicle Technologies, as part of the High Temperature Materials Laboratory User Program, Oak Ridge National Laboratory, managed by UT-Batelle, LLC, for the U.S. Department of Energy under contract number DE-AC05-00OR22725.

Based in part on the thesis submitted by Z. Chen for the M.S. Degree in Materials Engineering, Purdue University, West Lafayette, Indiana, 2003.

[†]Author to whom correspondence should be addressed. e-mail: rtrice@purdue.edu

of 7.6YSZ co-doped with rare earth elements (La, Nd, Sm, Gd, Y, and Yb). The authors found that the phase stability increased systematically as the size of the rare earth cation decreased for both single and co-doped compositions. In the research reported here, an approach similar to Levi and co-workers to limit the partitioning kinetics of the as-sprayed, metastable phase is investigated. However, in this study, we focus on preparing *plasma-sprayed* coatings made from co-doped 7.6YSZ or 12 mol% CeO_2–ZrO_2 (12CeSZ) powders to stabilize the t'-ZrO_2 phase. The co-dopants investigated included Ca^{2+} or Yb^{3+} ions.

II. Experimental Procedure

(1) Co-Dopant Infiltration and Coating Preparation

Two partially stabilized zirconia-based powders were investigated including one with 7.6 mol% $YO_{1.5}$ added as stabilizer (T14841/ZRO-236, Praxair Surface Technologies, Indianapolis, IN), and one containing 12 mol% CeO_2 (ZRO-248, Praxair Surface Technologies). These will be referred to as 7.6YSZ and 12CeSZ, respectively. Both 7.6YSZ and 12CeSZ powders were spray dried, with each powder comprising hundreds of particles <10 μm in diameter to form a porous structure. The diameters of 7.6YSZ and 12CeSZ powders were $\sim$100 μm, with some powders finer than this being observed.

Co-dopants of either Ca^{2+} or Yb^{3+} were incorporated into the spray-dried powders by infiltrating them with solutions containing the desired impurity. These two co-dopants were chosen because of their relative ionic radius as compared with the Y^{3+} stabilizer: Ca^{2+} is larger and Yb^{3+} is smaller.[14] The infiltrant was prepared by dissolving hydrated salts of either $Ca(NO_3)_2$ (Stock # 30482, Calcium Nitrate, Alfa Aesar, Ward Hill, MA) or $Yb(NO_3)_3$ (Stock # 12901, Ytterbium Nitrate, Alfa Aesar) in ethanol. The molar amount of the dopants added was such that they would substitute 2% or 5% of the total cation sites in the powder to be infiltrated. The seven different compositions presently studied are listed in Table I. The co-dopant solution was poured into a beaker with the powders, and the resulting slurry was subjected to a vacuum of 3 Pa for 1 h. The slurry was then dried, stirring occasionally at 80°C to evaporate the ethanol. The resultant paste was moved into an alumina crucible and calcined at 1100°C for 2 h. The loosely agglomerated powders were broken up mechanically prior to spraying, and sieved through an aperture of 150 μm.

The 7.6YSZ, 12CeSZ, and co-doped powders were plasma sprayed (a Praxair SG-100 gun (Praxair, Danbury, CT) with a 730 anode, 729 cathode and a 112 gas injector were used) at Ames Laboratory to form coatings for investigation. The spray parameters used for all powders are listed in Table II; these parameters were not optimized for each powder type. Substrates of two geometries were used: a copper plate of 102 mm $\times$ 76 mm $\times$ 5 mm and a 203 mm long copper tube with an outer diameter of 9.5 mm and an inner diameter of 7.9 mm. Coatings removed from the cylindrical substrate were used for dilatometry studies; coatings removed from flat substrates were used in all other investigations. The substrates were grit blasted with 24-grit Al_2O_3 at 5.5×10^5 Pa prior to coating. Air jets were used to cool the substrates while plasma spraying, and $\sim$30 spray cycles were used for each coating. The copper substrate was removed via a 1 h soak in HNO_3 to create either flat (i.e. from the plate) or cylindrical coatings (i.e. from the tube) for study. The amount of co-dopant incorporated into the coating was measured via mass spectroscopy techniques (NSL Analytical Services Inc., Cleveland, OH) on pulverized coatings.

(2) Coating Characterization

The bulk density and open porosity of the as-sprayed coatings were measured using the Archimedes method.[15] Approximately 1 g of specimen was used for each measurement. The accuracy of the scale was within 0.001 g.

Cross-sectional transmission electron microscopy (TEM) samples of as-sprayed 2Yb/7.6YSZ and 2Yb/12CeSZ were prepared using a tripod polisher (South Bay Technology, Santa Clara, CA). Both sides of each specimen were polished progressively using a sequence of diamond-coated polishing films until the thin end of the specimen began to recede. After the specimen was mounted on a nickel grid, an ion mill was used to further thin the specimen to electron transparency (model DMP 600, Gatan Ion Mill, Gatan Inc., Pleasanton, CA). TEM was carried out at Oak Ridge National Laboratory using a Hitachi HF2000 FEG-TEM (Hitachi High Technologies, Inc., Tokyo, Japan) equipped with a Thermo Electron Corporation electron-dispersive spectrometer (EDS) at 200 kV. EDS was used to measure the relative concentration of ytterbium content in 2Yb/7.6YSZ and 2Yb/12CeSZ within grains and across grain boundaries. The probe size was $\sim$2 nm in diameter.

The phase stability of as-sprayed and heat-treated coatings was investigated using X-ray diffraction (XRD; Siemens D500 Kristalloflex, Karlsruhe, Germany) with Cu$K\alpha$ radiation. Coatings of all compositions studied were heat treated at 1200°C for 10 and 100 h; the 2Yb/7.6YSZ coating was further heat treated at 1200°C for 400 h.

All seven coatings were analyzed for 2θ values of 20°–80° at a scan speed of 6°/min. The yttria-stabilized coatings were further investigated for 2θ values of 72°–76° at a scan speed of 0.5°/min to detect partitioning of the t'-ZrO_2 phase.[7,16] Deconvolution of the XRD peaks was performed using Rietveld analysis (TOPAS Software, Bruker AXS GmbH, Karlsruhe, Germany). For CeSZ coatings, 2θ values of 26°–34° were investigated at a scan speed of 1°/min. The integrated area intensity of {111} monoclinic and tetragonal/cubic phase was deconvoluted using Rietveld analysis. The volume ratio of the monoclinic phase to tetragonal/cubic phase in CeSZ was calculated using the following equation[12]:

$$\frac{V_m}{V_{t+c}} = 1.39\left[\frac{I_m(11\bar{1}) + I_m(111)}{I_{t+c}(111)}\right] \quad (1)$$

where V_m and V_{t+c} are the volume fraction of monoclinic phase and tetragonal+cubic phase; I_m and I_{t+c} are the integrated area intensity of the monoclinic phase and $t+c$ phase, respectively.

The shrinkage behavior of 12 mm tall stand-alone cylindrical coatings was characterized using a dilatometer (Orton 1600D push-rod type dilatometer, Orton Ceramic Foundation, Westerville, OH). Each sample was heated up at 10°C/min ramp to 1400°C and held for 5 h. A probe that can move in the axial direction was in contact with the sample to follow the expansion or contract upon heating. Data of temperature, probe displace-

Table I. Overview of the Coatings Investigated in the As-Sprayed Condition

Coating designation	Tested dopant concentration (mol%)‡	Average thickness (μm)	Bulk density (g/cm^3)	Open porosity (%)
7.6YSZ	0.24 Ca†	$\sim$550	5.23±0.07	10.5±0.9
2Ca/7.6YSZ	1.75 Ca	$\sim$400	5.08±0.06	11.3±0.3
5Ca/7.6YSZ	4.10 Ca	$\sim$390	4.96±0.04	13.7±1.8
2Yb/7.6YSZ	2.69 Yb	$\sim$480	5.14±0.02	12.4±0.9
12CeSZ	0.11 Ca†	$\sim$570	5.59±0.03	8.0±0.6
2Ca/12CeSZ	1.43 Ca	$\sim$640	5.65±0.01	7.5±0.1
2Yb/12CeSZ	2.18 Yb	$\sim$490	5.57±0.02	9.1±0.9

†As an impurity in the starting powder. ‡NSL Analytical Services Inc. 7.6YSZ, 7.6 mol% $YO_{1.5}$–ZrO_2; 12CeSZ, 12 mol% CeO_2–ZrO_2.

Table II. Parameter of Plasma Spraying

Current (A)	900
Volts (at gun)	41.3
Arc gas (scfh)	54 (Ar)
Aux gas (scfh)	44 (He)
Carrier gas (scfh)	13 (Ar)
Powder feed rate (rpm)	1.5
Stand off distance (cm)	10.0

scfh, standard cubic feet per hour.

ment, and time were collected *in situ* by a computer. Shrinkage of the specimen was obtained by subtracting the thermal expansion of the apparatus and that of the sample being tested from probe displacement.

(3) Thermal Conductivity Measurements

The thermal conductivity, k_{th}, in units of W/m/K, as a function of temperature for each of the coatings was calculated using the following equation:

$$k_{th}(T) = \alpha(T) \cdot c_p(T) \cdot \rho \cdot 100$$

where $\alpha(T)$ is the thermal diffusivity as a function of temperature in units of cm^2/s, $c_p(T)$ is the specific heat as a function of temperature in units of J/g/K, and ρ is the as-sprayed density (g/cm^3) of the coating being investigated.

Thermal diffusivity (Flashline 5000 Thermal Diffusivity System, Anter Corporation, Pittsburgh, PA), α, was measured as a function of temperature using the laser flash method at the Oak Ridge National Laboratory. A detailed description of the system setup and measurement technique has been published elsewhere.[17] Disk-shaped samples, 12.7 mm in diameter, were used for all measurements. The disk samples were spray coated with a thin layer of colloidal graphite to ensure similar surface radiation characteristics in all samples prior to testing. Thermal diffusivity data were collected every 100°C from 100° to 1200°C. Specimens were tested in an aluminum furnace from 100° to 500°C and continued in a graphite furnace from 700° to 1200°C in a nitrogen atmosphere. An InSb detector was used in the low-temperature furnace and a silicon infrared detector was used in the high-temperature furnace. Three measurements were taken for each sample at each temperature and averaged. At least two samples of each coating were tested. The time–temperature curves were analyzed by the method of Clark and Taylor,[18] which takes into account radiation losses and uses the heating part of the curve to calculate thermal diffusivity. Specific heat as a function of temperature, $c_p(T)$, was measured from 25° to 1200°C at a heating rate of 20°C/min using a differential scanning calorimeter (Netzsch Instruments DSC 404C, Burlington, MA).

III. Results and Discussion

(1) Characterization of As-Sprayed 7.6YSZ and 12CeSZ Coatings

The measured co-dopant composition and physical properties of all as-sprayed coatings are summarized in Table I. The actual co-dopant concentrations were found to be within $\pm 35\%$ of the expected concentrations for all samples; these differences may arise from the hydration/dehydration of the reactant chemicals. Coating depositions for all coatings were between 13 and 20 μm/pass. Densities were close to ~ 5 g/cm^3 for co-doped and baseline 7.6YSZ coatings and ~ 5.6 g/cm^3 for co-doped and baseline 12CeSZ coatings. Except for 2Ca/12CeSZ, the co-doped as-sprayed coatings displayed more open porosity than their baseline counterparts.

(2) TEM and EDS Investigations of 2Yb/7.6YSZ and 2Yb/12CeSZ Coatings

Investigation of both 2Yb/7.6YSZ and 2Yb/12CeSZ as-sprayed coatings in cross-section revealed typical plasma-sprayed microstructures,[19,20] with lamellae structures composed of columnar grains observed. Intralamellar microcracks, located between grains, and lenticular-shaped interlamellar pores between two adjacent lamellae were also observed. Also, preliminary studies using high-resolution imaging of grain boundaries from either 2Yb/7.6YSZ or 2Yb/12CeSZ coatings showed no evidence of either an amorphous or crystalline grain boundary phase. In the current work, the location of Yb atoms in the grains and between their boundaries was investigated.

Figure 1 presents a TEM micrograph and corresponding EDS analysis from a region within a lamella of a 2Yb/7.6YSZ sample. As indicated with circles in the micrograph, analysis was performed at two regions inside each grain (points A and D), and at a grain boundary (point C). Note that the circles indicated on the image are to indicate probe location and that the actual probe size is much smaller than the diameter of the circle. The highest intensity peak corresponded to Zr-L_α; an Yb-M_α peak was also evident in each location in the inset EDS spectra. It was found that the intensity ratio of the Yb-M_α and Zr-L_α peaks was approximately the same whether the location of probe was inside the grain or across the grain boundary. This would suggest that no segregation of Yb occurs at the grain boundary. Four other random regions were examined; despite slight variation of Yb content from region to region, no enrichment of Yb was detected at the grain boundary.

EDS and TEM analysis of 2Yb/12CeSZ revealed similar results. Figure 2 shows EDS spectra taken in a typical columnar grains area. EDS revealed that grain interior A, C and grain boundary B, D had the same small Yb peaks. Probing at other regions revealed no grain boundary segregation either.

Although grain boundary segregation is extensively observed in zirconia materials,[21,22] the conditions for this to occur are not well known. In our study, coatings were deposited on a substrate and cooled rapidly. McPherson and Shafer[23] has estimated the cooling rate to be as high as $\sim 10^6$ K/s. It is possible that the defect equilibrium does not have sufficient time to set up. As a result, no segregation was observed. Annealing at high temperature followed by a slow cooling may allow redistribution of cations and oxygen vacancies near grain boundaries driven by the space charge potential.

In summary, EDS results showed regions where Yb concentrations varied from a significant to a trace amount. The variation was probably because of the different diffusion distances of Yb. Since the spray-dried powder was composed of individual particles, and the co-dopant is added to the particles from the exterior, it was expected that particle exteriors would have a higher Yb concentration than the interior. While it was clear that a variation of Yb content did exist from region to region, in the same region, however, no evident variation was noted between grain interiors and grain boundaries within limits of the testing resolution.

(3) Linear Shrinkage Measurement

Four samples for each of 7.6YSZ, 12CeSZ, 2Yb/7.6YSZ, and 2Yb/12CeSZ were tested using a dilatometer. The final shrinkage at the end of the 5 h hold at 1400°C was recorded. The average and range of final shrinkage are listed in Table III. It was observed that the linear shrinkage difference between coatings is within the testing error. Therefore, no significant difference exists in the shrinkage behavior among the co-doped coatings and their baseline counterpart.

(4) Phase Stability of Co-Doped 7.6YSZ Coatings

Figure 3 shows the XRD peaks for both the as-sprayed co-doped and baseline 7.6YSZ coatings. For the 7.6YSZ, 2Ca/7.6YSZ, and 2Yb/7.6YSZ coatings, a non-equilibrium composition tetragonal phase was observed. This phase, identified presently as t'-ZrO_2, typically has ~ 7.6 mol% $YO_{1.5}$ and if applicable, the co-dopant ion, in solid solution with the ZrO_2. The 5Ca/7.6YSZ sample was completely cubic zirconia of a non-equilibrium composition (c'-ZrO_2).

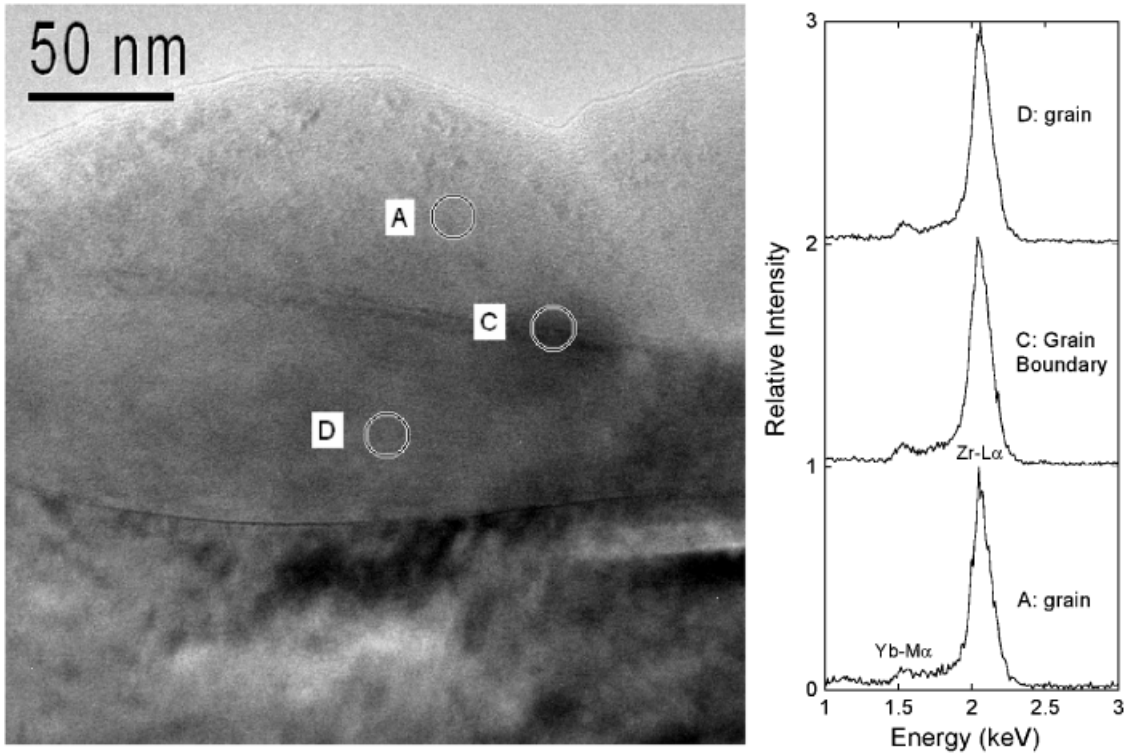

Fig. 1. Electron-dispersive spectrometer spectra and corresponding transmission electron microscopy micrograph showing probe location in a 2Yb/7.6 mol% $YO_{1.5}$–ZrO_2 coating. Note that because the Zr-L and Y-L energies are very similar, it is difficult to resolve these two peaks. However, inspection of the X-ray spectrum from 1–20 keV showed a Y-K^{α} line close to 14.9 keV; the ratio of yttrium peak height to zirconium peak height for their respective K^{α} lines did not vary substantially for points A, B, or C.

After a 10 h heat treatment at 1200°C, not shown, only the t'-ZrO_2 phase was observed in 7.6YSZ, 2Ca/7.6YSZ, and 2Yb/7.6YSZ; however, there was some shifting of the (004) peak of each coating composition to smaller 2Θ values. In 5Ca/7.6YSZ, the emergence of a tetragonal zirconia phase was observed. Thus, it appears that increasing the amount of Ca^{2+} co-dopant decreases the stability of 7.6YSZ.

Figure 4 presents the XRD peaks of the co-doped and baseline 7.6YSZ coatings after 100 h at 1200°C. Note that c-ZrO_2 has begun to form in the 7.6YSZ and 2Ca/7.6YSZ coatings. The excess yttria in the t'-ZrO_2 phase forms the c-ZrO_2 phase, and its presence is a good indicator that destabilization of the t'-ZrO_2 phase is beginning. It should be noted that while the original metastable t'-ZrO_2 phase has begun to partition into an yttria-rich c-ZrO_2 phase, the remaining tetragonal phase, while it has less than 7.6 mol% $YO_{1.5}$, is still "non-transformable" in that its composition is greater than would be predicted by the equilibrium phase diagram. This was verified by XRD where no m-ZrO_2 was detected.

A c-ZrO_2 peak was also observed as in the 2Ca/7.6YSZ sample after 100 h at 1200°C. Thus, Ca^{2+} co-doping does not appear

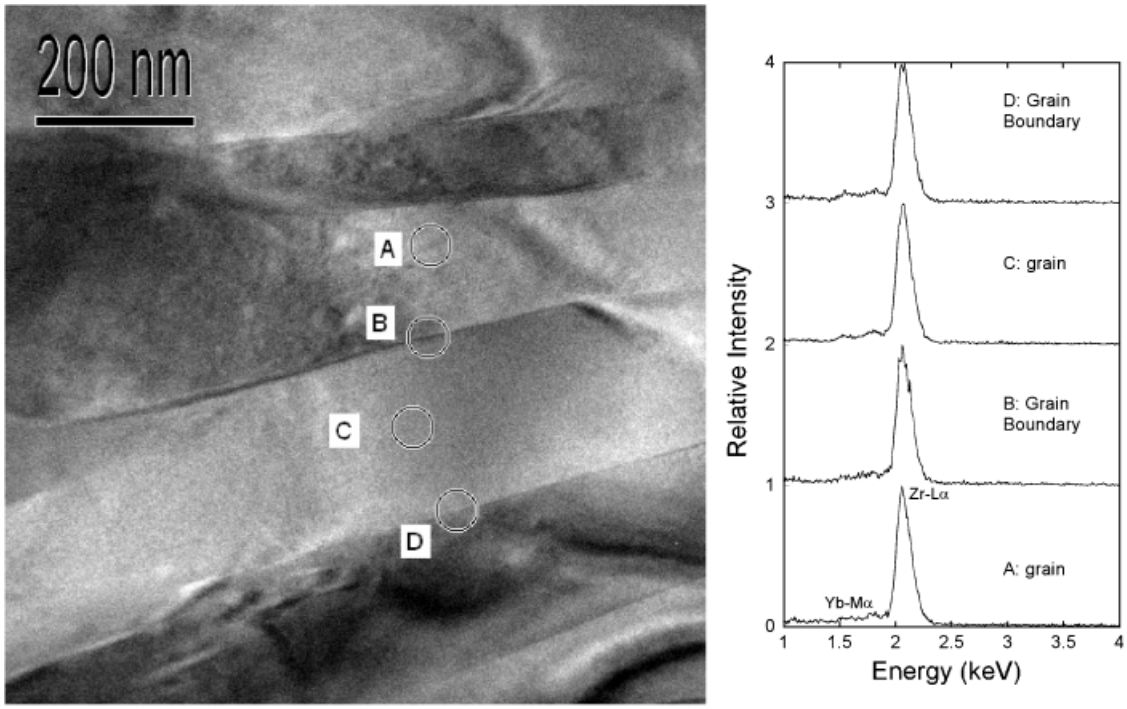

Fig. 2. Electron-dispersive spectrometer spectra and corresponding micrographs showing probe location in a 2Yb/12CeSZ coating.

Table III. Linear Shrinkage After 300 min at 1400°C

Coating	Linear shrinkage after 300 min at 1400°C (%)
7.6YSZ	0.56±0.17
2Yb/7.6YSZ	0.68±0.23
12CeSZ	0.63±0.28
2Yb/12CeSZ	0.66±0.24

7.6YSZ, 7.6 mol% $YO_{1.5}$–ZrO_2; 12CeSZ, 12 mol% CeO_2–ZrO_2.

to stabilize the t'-ZrO_2 phase. However, no change in the phase assemblage of 2Yb/7.6YSZ coatings was observed after 100 h at 1200°C. The separation between (004) and (400) tetragonal phase became more evident with longer heat-treatment time. Thus, the resistance to partitioning of the t'-ZrO_2 phase seemed to be enhanced by co-doping with Yb^{3+}. Furthermore, a heat treatment of 400 h at 1200°C on the 2Yb/7.6YSZ revealed that some c-ZrO_2 has formed, but no m-ZrO_2 was observed. The 5Ca/7.6YSZ coating was further characterized by destabilization of the c'-ZrO_2 phase.

According to the equilibrium Y_2O_3–ZrO_2 binary phase diagram[24] and the CaO–Y_2O_3–ZrO_2[25] (at 1250°C) and Yb_2O_3–Y_2O_3–ZrO_2[26] (at 1200°C) ternary phase diagrams, all four YSZ-based coatings, 7.6YSZ, 2Ca/7.6YSZ, 5Ca/7.6YSZ, and 2Yb/7.6YSZ, lie in the cubic and tetragonal two-phase field. The ternary compositions of 2Ca/7.6YSZ and 2Yb/7.6YSZ are both about in the middle of the tieline joining the equilibrium tetragonal and cubic boundary, and it may suggest a similar thermodynamic driving force for phase separation.[13]

In accordance with the phase diagrams, after 100 h heat treatment the phases in 7.6YSZ, 2Ca/7.6YSZ, and 5Ca/7.6YSZ were composed of tetragonal and cubic phases. Although it is difficult to determine whether the compositions of these phases are the equilibrium composition, phase separation of the as-sprayed coatings was evident. As previously stated, no phase separation was observed in the 100 h heat-treated 2Yb/7.6YSZ sample, indicating that phase separation in 2Yb/7.6YSZ is slower.

Phase separation in 7.6YSZ and 12CeSZ occurs via the diffusion of cations; the ionic radius of the relevant cations[22] for this study is as follows: $r_{Zr^{4+}} < r_{Yb^{3+}} < r_{Y^{3+}} < r_{Ca^{2+}}$. Since Ca^{2+} is larger in size than Yb^{3+}, it is expected to diffuse slower. However, 2Yb/7.6YSZ showed clear evidence of phase stabilization, while the 2Ca/7.6YSZ did not. Therefore, the slower phase separation in 2Yb/7.6YSZ cannot be explained by transport kinetics. And as suggested above, the thermodynamic driving force of 2Yb/7.6YSZ and 2Ca/7.6YSZ could be similar, and would not account for the difference either. Thus, it is most likely that the difference in phase stability between 2Ca/7.6YSZ and 2Yb/7.6YSZ arises from the coherency strains between the host and co-dopant ions in the structure. The larger co-dopant ions can increase the local distortion of the anion lattice and are believed to promote the nucleation of c-ZrO_2.[13] Therefore, it is expected that Yb^{3+} co-doping would accommodate distortion, while Ca^{2+} co-doping would induce more severe distortion because of the larger size mismatch with Zr^{4+} ions. A higher Ca^{2+} concentration induces more localized distortion and therefore more nucleation sites, which could explain why 5Ca/7.6YSZ began to partition after only 10 h at 1200°C.

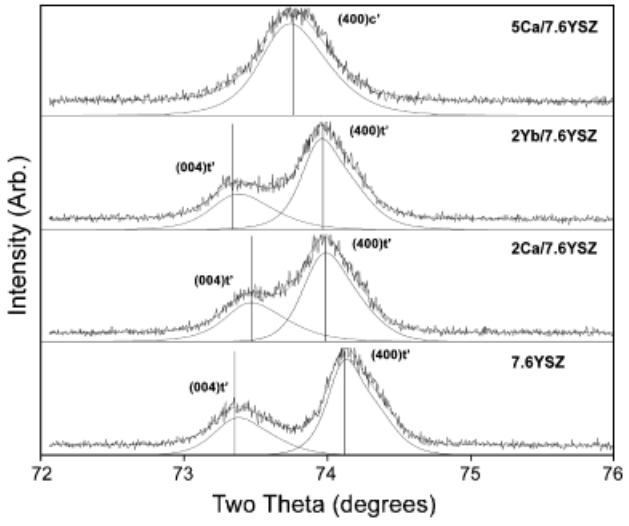

Fig. 3. Diffraction pattern of as-sprayed (a) 7.6 mol% $YO_{1.5}$–ZrO_2 (7.6YSZ), (b) 2Ca/7.6YSZ, (c) 5Ca/7.6YSZ, and (d) 2Yb/7.6YSZ for 2θ between 72° and 76°. All samples were pulverized prior to testing.

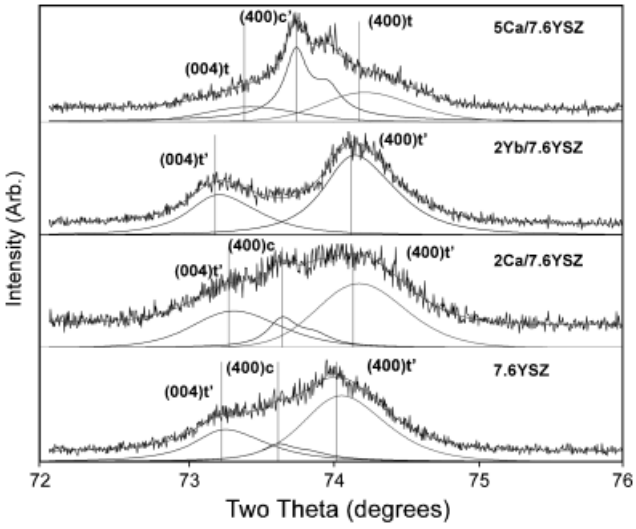

Fig. 4. Diffraction pattern of (a) 7.6 mol% $YO_{1.5}$–ZrO_2 (7.6YSZ), (b) 2Ca/7.6YSZ, (c) 5Ca/7.6YSZ, and (d) 2Yb/7.6YSZ after 100 h at 1200°C. All samples were pulverized prior to testing.

(5) Phase Stability of Co-Doped 12CeSZ Coatings

XRD peaks of as-sprayed 2Ca/12CeSZ and 2Yb/12CeSZ (not shown) resembled those of baseline 12CeSZ, consisting of mostly a single non-equilibrium composition tetragonal phase, along with some m-ZrO_2. After a 10 h heat treatment at 1200°C, a significant increase of m-ZrO_2 phase was present in all three compositions of coatings; the amount of the m-ZrO_2 phase further increased after a 100 h heat treatment. The increase of m-ZrO_2 volume fraction with heat-treatment time at 1200°C is summarized in Table IV. These quantitative data were acquired from deconvolution of integrated intensity of $(111)_m$ and $(111)_{t+c}$ peaks in the $2\theta = 26°$–$34°$ region according to Eq. (1). As-sprayed coatings all started with about 7–8 vol% of the m-ZrO_2 phase. After 100 h heat treatment, the m-ZrO_2 phase amount was as much as 88 vol% in 12CeSZ, and only 43 and 37 vol% in Ca^{2+} and Yb^{3+} co-doped coatings, respectively. This result suggests that co-doping may stabilize the as-sprayed tetragonal phase in ceria-stabilized zirconia, and therefore limit the tetragonal-to-monoclinic transformation.

(6) Thermal Conductivity Measurements

Figure 5 presents the thermal conductivity of as-sprayed baseline and co-doped 7.6YSZ coatings as a function of measure-

Table IV. Volume Fraction of Monoclinic Phase in As-Sprayed and 10 and 100 h Heat-Treated Samples of 12CeSZ, 2Ca/12CeSZ, and 2Yb/12CeSZ

	Vol% of m-ZrO_2 phase		
	As-sprayed	10 h at 1200°C	100 h at 1200°C
12CeSZ	8	84	88
2Ca/12CeSZ	8	33	43
2Yb/12CeSZ	7	36	37

Error in each measurement is ±2%. 12CeSZ, 12 mol% CeO_2–ZrO_2.

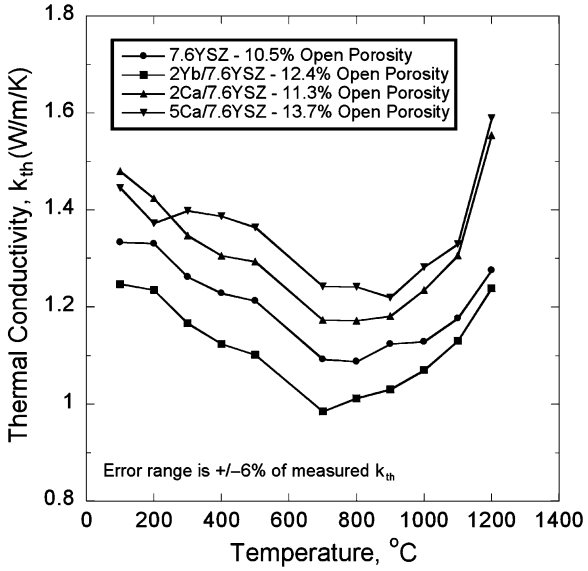

Fig. 5. Thermal conductivity of as-sprayed plasma-sprayed Yb^{3+} and Ca^{2+} co-doped 7.6 mol% $YO_{1.5}$–ZrO_2 (7.6YSZ) coatings at different measuring temperatures. The amount of open porosity in each coating is also indicated.

ment temperature. For all samples, it was observed that the conductivity decreases with temperature until it reaches ~700°C, and then increases through 1200°C. In the temperature range investigated, 2Yb/7.6YSZ exhibited a lower value of thermal conductivity than 7.6YSZ. However, co-doping with 2 and 5 mol% Ca (2Ca/7.6YSZ and 5Ca/7.6YSZ) resulted in coatings with higher k_{th} than the baseline 7.6YSZ coating. Ca^{2+} co-doped coatings also exhibited a more dramatic increase in k_{th} as the temperature increased beyond 1000°C.

Figure 6 shows the thermal conductivity of as-sprayed baseline and co-doped 12CeSZ coatings. Again, the Yb^{3+} co-doped coating demonstrated the lowest thermal conductivity among the three tested, and 2Ca/12CeSZ exhibited thermal conductivity comparable with the baseline 12CeSZ coating.

Defects play a critical role in reducing the intrinsic thermal conductivity of zirconia. In yttria-stabilized zirconia, the substitution of Zr^{4+} with Y^{3+} is accompanied by the creation of oxygen vacancies to maintain the electroneutrality of the lattice. One expects oxygen vacancies to be much stronger phonon scatterers than Y^{3+} cations, which have only a slightly different mass and size than Zr^{4+} cations. However, the concentration of oxygen vacancies is dependent on the concentration of Y^{3+} in zirconia. A theoretical calculation performed by Bisson *et al.*[27] predicts that the thermal conductivity of YSZ should decrease monotonically with increasing oxygen vacancy concentration; however, their k_{th} measurements on a YSZ single crystal showed that there was a minimum value for thermal conductivity at ap-

Table V. Calculated Oxygen Vacancy Concentration and Measured Open Porosity in Baseline and Co-Doped Coatings

Coating	Oxygen vacancy concentration (mol%)	Open porosity (%)
7.6YSZ	1.9	10.5
2Ca/7.6YSZ	2.9	11.3
5Ca/7.6YSZ	4.4	13.7
2Yb/7.6YSZ	2.4	12.4
12CeSZ	0	8.0
2Ca/12CeSZ	1	7.5
2Yb/12CeSZ	0.5	9.1

7.6YSZ, 7.6 mol% $YO_{1.5}$–ZrO_2; 12CeSZ, 12 mol% CeO_2–ZrO_2.

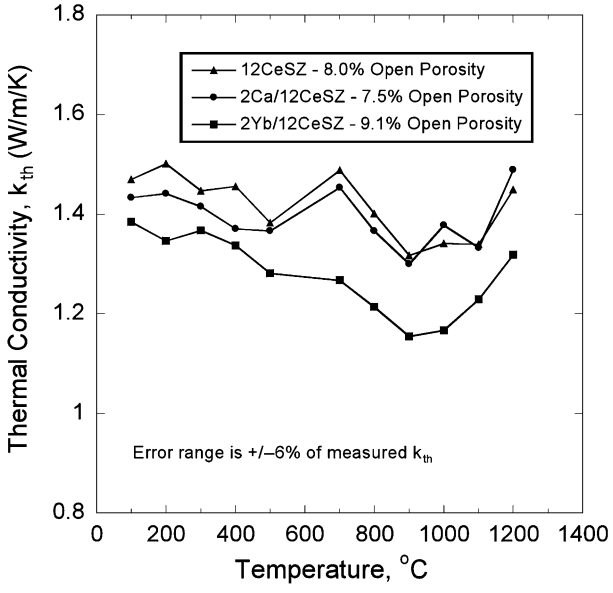

Fig. 6. Thermal conductivity of as-sprayed Yb^{3+} and Ca^{2+} co-doped 12 mol% CeO_2–ZrO_2 (12CeSZ) coatings at different measuring temperatures. The amount of open porosity in each coating is also indicated.

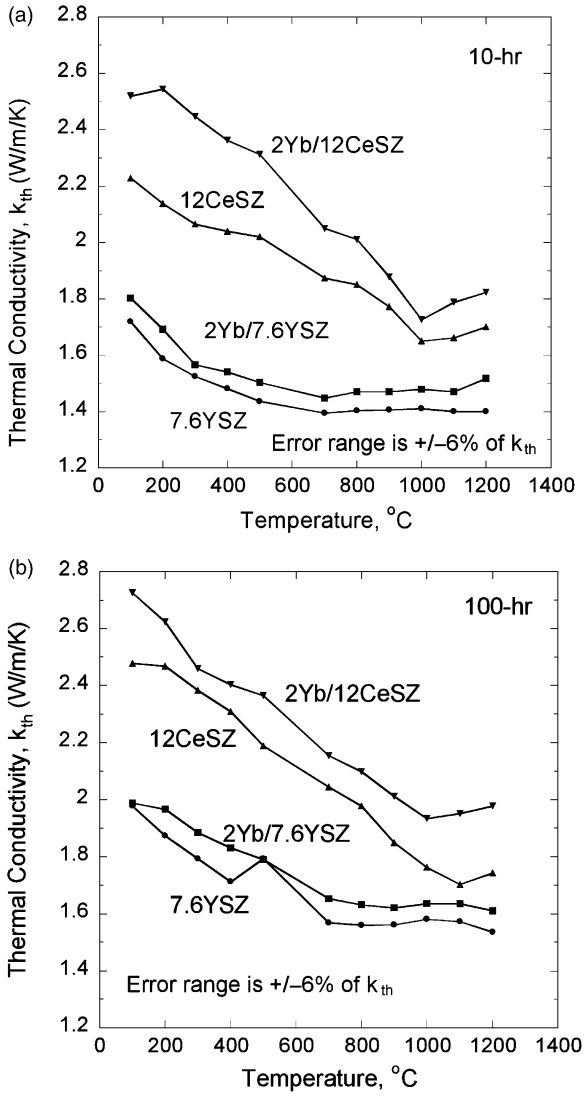

Fig. 7. The thermal conductivity of baseline and Yb^{3+} co-doped 7.6 mol% $YO_{1.5}$–ZrO_2 (7.6YSZ) and 12 mol% CeO_2–ZrO_2 (12CeSZ) coatings after (a) 10 h and (b) 100 h heat treatments at 1200°C.

proximately a 5 mol% oxygen vacancy concentration. They argued that the increase in k_{th} beyond 5 mol% oxygen vacancies was because of the local ordering of the point defects. Recent research on defect structure of cubic YSZ supported this hypothesis.[28]

The calculated oxygen vacancy concentrations for the baseline and co-doped coatings are listed in Table V, along with the measured open porosity values. We observed that the as-sprayed 7.6YSZ and 2Yb/7.6YSZ fit the above-mentioned trend, i.e. they demonstrated a decrease in thermal conductivity with increased oxygen vacancy concentration. It should also be noted that the decrease in thermal conductivity observed in Fig. 5 could also be attributed to the higher porosity observed in the 2Yb/7.6YSZ coating. A previous study by Trice *et al.*[29] showed that a 2% increase in porosity resulted in an $\sim$0.1 J/m/K decrease in thermal conductivity. However, while the Ca^{2+}-doped samples have a larger concentration of oxygen vacancies and greater open porosity, they exhibited greater thermal conductivity as compared with the 7.6YSZ coating. Therefore, some factors other than oxygen vacancy concentration or porosity should account for this behavior. One of these factors could be point defect clustering caused by the coherency effect of different dopant species. Some literature suggested such a link between thermal conductivity and co-doping, but the fundamental aspect is not yet clear.[30]

Figure 7(a) and (b) shows a comparison of the thermal conductivity of 7.6YSZ and 12CeSZ baseline and Yb^{3+} co-doped coatings after 10 and 100 h heat treatments at 1200°C. It was found that unlike the as-sprayed coatings, the heat-treated Yb^{3+} co-doped coatings show no advantage over either baseline 7.6YSZ or 12CeSZ coatings. In general, the CeSZ-based coatings have higher thermal conductivity than YSZ-based coatings, probably because the latter contains more oxygen vacancies that tend to scatter the lattice waves.

IV. Conclusions

Co-dopants of either Yb^{3+} or Ca^{2+} were successfully incorporated in 7.6YSZ and 12CeSZ coatings by infiltrating porous spray-dried powders with salt solutions containing the appropriate co-dopant species prior to plasma spraying. No Yb^{3+} segregation was detected at the grain boundary of either as-sprayed 2Yb/7.6YSZ or 2Yb/12CeSZ coatings. Based on the dilatometer measurements, Yb^{3+} co-doped coatings did not demonstrate any difference in shrinkage behavior as compared with baseline 7.6YSZ and 12CeSZ coatings.

XRD results show that the as-sprayed 7.6YSZ, 2Ca/7.6YSZ, and 2Yb/7.6YSZ coatings comprised of non-transformable, non-equilibrium composition t'-ZrO_2. Both 7.6YSZ and 2Ca/7.6YSZ partitioned into c-ZrO_2 and t-ZrO_2 after a 100-h heat treatment at 1200°C; however, no m-ZrO_2 was observed. The 2Yb/7.6YSZ coating retained a single t'-ZrO_2 phase after a 100 h heat treatment. Thus, it can be concluded that 2 mol% Yb^{3+} co-dopant increases the stability of the t'-ZrO_2 phase as compared with the baseline coating made from 7.6YSZ. The as-sprayed 5Ca/7.6YSZ was a single c'-ZrO_2 phase, but began to partition after a 10 h heat treatment at 1200°C. The volume fraction of m-ZrO_2 in 12CeSZ was estimated to be 88% after a 100 h heat treatment. Yb^{3+} and Ca^{2+} co-doping limited the $t \rightarrow m$ phase transformation in 12CeSZ, with only 37% and 43% monoclinic phase observed, respectively, after a 100 h heat treatment at 1200°C.

The thermal conductivity of plasma-sprayed 7.6YSZ is lower than that of 12CeSZ, probably because the former contains more oxygen vacancies that tend to scatter the lattice waves. As-sprayed 2Yb/7.6YSZ and 2Yb/12CeSZ coatings had lower thermal conductivity than their undoped counterparts. The decrease in thermal conductivity of Yb^{3+} co-doped coatings is attributed to both an increase in oxygen vacancies or more porous structure. However, after heat treating for 10 and 100 h at 1200°C, Yb^{3+} co-doped, as-sprayed 2Ca/7.6YSZ, 5Ca/7.6YSZ, and 2Ca/12CeSZ showed little or no effect in decreasing the thermal conductivity from the baseline coatings.

References

[1]R. A. Miller, "Current Status of Thermal Barrier Coatings—An Overview," *Surf. Coat. Technol.*, **30**, 1–11 (1987).

[2]S. Sodeoka, M. Suzuki, S. K. Ueno, H. Sakuramoto, T. Shibata, and M. Ando, "Thermal and Mechanical Properties of ZrO_2–CeO_2 Plasma-Spray Coatings," *J. Therm. Spray Technol.*, **6** [3] 361–7 (1997).

[3]J. Wilden, M. Wank, H. D. Steffens, and M. Brune, "New Thermal Barrier Coating System for High Temperature Applications," *Proc. Int. Thermal Conf.*, **2**, 1669–73 (1998).

[4]R. Hillery, *Coatings for High Temperature Structural Materials*. National Academy Press, Washington, DC, 1996.

[5]A. Rabiei and A. Evans, "Failure Mechanisms Associated with the Thermally Grown Oxide in Plasma-Sprayed Thermal Barrier Coatings," *Acta Mater.*, **48** [15] 3963–76 (2000).

[6]A. Freborg, B. Ferguson, W. Brindley, and G. Petrus, "Modeling Oxidation Induced Stresses in Thermal Barrier Coatings," *Mater. Sci. Eng. A*, **A245** [2] 182–90 (1998).

[7]K. Muraleedharan, J. Subrahmanyam, and S. B. Bhaduri, "Identification of t′ Phase in ZrO_2-7.5 wt.% Y_2O_3 Thermal Barrier Coatings," *J. Am. Ceram. Soc.*, **71** [5] C226–7 (1998).

[8]H. G. Scott, "Phase Relationships in the ZrO_2–Y_2O_3 Systems," *J. Mater. Sci.*, **10** [9] 1527–35 (1975).

[9]N. R. Rebollo, O. Fabrichnaya, and C. G. Levi, "Phase Stability of Y+Gd Co-Doped Zirconia," *Z. Metallkd.*, **94** [3] 163–70 (2003).

[10]J. Ilavsky and J. K. Stalick, "Phase Composition and its Changes During Annealing of Plasma-Sprayed YSZ," *Surf. Coat. Technol.*, **127**, 120–9 (2000).

[11]J. Ilavsky, J. K. Stalick, and J. Wallace, "Thermal-Spray Yttria-Stabilized Zirconia Phase Changes During Annealing"; pp. 1185–9 in Proceedings of International Thermal Spray Conference, Montreal, 2000.

[12]E. Y. Lee, Y. Sohn, S. K. Jha, J. W. Holmes, and R. D. Sisson Jr., "Phase Transformation of Plasma-Sprayed Zirconia-Ceria Thermal Barrier Coatings," *J. Am. Ceram. Soc.*, **85** [8] 2065–71 (2002).

[13]N. R. Rebollo, A. S. Gandhi, and C. G. Levi, "Phase Stability Issues in Emerging TBC Systems"; pp. 431–42 in *High Temperature Corrosion and Materials Chemistry IV. Electrochemical Society Proceedings*, **Vol. PV-2003-16**, Edited by E. Opila, P. Hou, T. Maruyama, B. Pieraggi, M. McNallan, D. Shifler, and E. Wuchina. Electro-Chemical Society, Paris, 2003.

[14]Y. M. Chiang, D. Birnie III, and W. D. Kingery, *Physical Ceramics: Principles for Ceramic Science and Engineering*. Wiley Publishers, New York, 1997.

[15]ASTM C373-88, *Standard Test Method for Water Absorption, Bulk Density, Apparent Porosity and Apparent Specific Gravity of Fired Whiteware Products (Reapproved 1999)*. ASTM, Philadelphia, 1999.

[16]P. A. Langjahr, R. Oberacker, and M. J. Hoffman, "Long-Term Behavior and Application Limits of Plasma-Sprayed Zirconia Thermal Barrier Coatings," *J. Am. Ceram. Soc.*, **84** [6] 1301–8 (2001).

[17]H. Wang, R. B. Dinwiddie, and P. S. Gaal, "Multiple Station Thermal Diffusivity Instrument"; pp. 119–27 in *Thermal Conductivity*, **Vol. 23**, Edited by K. E. Wilkes, R. B. Dinwiddie, and R. S. Graves. Technomic Publishing, Basel, 1996.

[18]L. M. Clark III and R. E. Taylor, "Radiation Loss in the Flash Method for Thermal Diffusivity," *J. Appl. Phys.*, **46** [2] 714–9 (1975).

[19]R. McPherson, "A Review of Microstructure and Properties of Plasma-Sprayed Ceramic Coatings," *Surf. Coat. Technol.*, **39/40**, 173–81 (1989).

[20]R. W. Trice, Y. J. Su, J. R. Mawdsley, K. T. Faber, A. R. De Arellano-López, H. Wang, and W. D. Porter, "Effect of Heat Treatment on Phase Stability, Microstructure, and Thermal Conductivity of Plasma-Sprayed YSZ," *J. Mater. Sci.*, **37**, 2359–65 (2002).

[21]J. A. Hines, Y. Ikuhara, A. H. Chokshi, and T. Sakuma, "The Influence of Trace Impurities on the Mechanical Characteristics of a Superplastic 2 mol% Yttria Stabilized Zirconia," *Acta Mater.*, **46** [15] 5557–68 (1998).

[22]S. Hwang and I. Chen, "Grain Size Control of Tetragonal Zirconia Polycrystals Using the Space Charge Concept," *J. Am. Ceram. Soc.*, **73** [11] 3269–77 (1990).

[23]R. McPherson and B. Shafer, "Interlamellar Contact in Plasma-Sprayed Coatings," *Thin Solid Films*, **97**, 201–4 (1982).

[24]R. Stevens, *Zirconia and Zirconia Ceramics*. Magnesium Elektron Ltd, Manchester, 1986.

[25]E. R. Andrievskaya, I. E. Kir'yakova, and L. M. Lopato, "Phase-Equilibria in the Systems HfO_2–Y_2O_3–CaO and ZrO_2–Y_2O_3–CaO at 1250°C," *Inorg. Mater.*, **27** [10] 1839–44 (1991).

[26]G. S. Corman and V. S. Stubican, "Phase-Equilibria and Ionic-Conductivity in the System ZrO_2–Yb_2O_3–Y_2O_3," *J. Am. Ceram. Soc.*, **68** [4] 174–81 (1985).

[27]J. Bisson, D. Fournier, M. Poulain, O. Lavigne, and R. Mevrel, "Thermal Conductivity of Yttria–Zirconia Single Crystals, Determined with Spatially Resolved Infrared Thermography," *J. Am. Ceram. Soc.*, **83** [8] 1993–8 (2000).

[28]J. P. Goff, W. Hayes, S. Hull, M. T. Hutchings, and K. N. Clausen, "Defect Structure of Yttria-Stabilized Zirconia and its Influence on the Ionic Conductivity at Elevated Temperatures," *Phys. Rev. B*, **59** [22] 14202–19 (1999).

[29]R. W. Trice, Y. J. Su, K. T. Faber, H. Wang, and W. Porter, "The Role of NZP Addition in Plasma-Sprayed YSZ: Microstructure, Thermal Conductivity and Phase Stability Effects," *Mater. Sci. Eng. A*, **A272** [2] 284–91 (1999).

[30]D. Zhu and R. A. Miller, "Thermal Conductivity and Sintering Behavior of Advanced Thermal Barrier Coatings," *Ceram. Eng. Sci. Proc.*, **23** [4] 457–68 (2002). □